Nanoscale Res Lett (2010) 5:442–447
DOI 10.1007/s11671-009-9503-7

NANO EXPRESS

Dysprosium-Catalyzed Growth of Single-Walled Carbon Nanotube Arrays on Substrates

Yong Qian · Chunyan Wang · Bin Huang

Received: 14 October 2009 / Accepted: 20 November 2009 / Published online: 29 November 2009

Abstract In this letter, we report that dysprosium is an effective catalyst for single-walled carbon nanotubes (SWNTs) growth via a chemical vapor deposition (CVD) process for the first time. Horizontally superlong well-oriented SWNT arrays on SiO_2/Si wafer can be fabricated by EtOH-CVD under suitable conditions. The structure and properties are characterized by scanning electron microscopy, transition electron microscopy, Raman spectroscopy and atomic force microscopy. The results show that the SWNTs from dysprosium have better structural uniformity and better conductivity with fewer defects. This rare earth metal provides not only an alternative catalyst for SWNTs growth, but also a possible method to generate high percentage of superlong semiconducting SWNT arrays for various applications of nanoelectronic device.

Keywords Dysprosium · Chemical vapor deposition · Single-walled carbon nanotube

Introduction

Single-walled carbon nanotubes (SWNTs) have attracted enormous attention due to their unique structures and excellent properties [1–4] since their discovery [5]. Several approaches [5–8] have been developed for the production of SWNTs, among which the catalyst plays an important role in the chemical vapor deposition (CVD) process of SWNTs [9]. It is generally accepted that the nanoscaled catalyst particles act as the initiating centers, and the SWNTs grow out from them via a vapor–liquid–solid (VLS) mechanism [10]. The Fe-family elements are known to be the most common catalysts. Experimental [11] and theoretical [12, 13] studies all show their high catalytic activities. However, in the past 3 years, many other metals such as Ag, Pd, Au, Cu, Rh and Pb [14–19], semiconductors such as Si and Ge [16], carbides such as SiC [16], Fe_3C [20] and more recently Mg, Mn, Cr, Sn and Al [21, 22] have been reported to be active for SWNTs growth. These materials were regarded as inactive catalysts for the growth of CNTs in the past. Therefore, these findings challenge the traditional thinking about the growth of CNTs and the role of the catalysts. Furthermore, different types of catalysts will provide more chance to understand the relationship between the catalyst and the structures of the SWNTs and thus may find out the approach for selective growth of semiconducting SWNTs (s-SWNTs) or metallic SWNTs (m-SWNTs).

In situ growth of horizontally well-aligned SWNT arrays up to a centimeter scale on suitable substrates is a critical step for large-scale, low-cost fabrication of the SWNT-based electronic devices, especially on commercial silicon wafer substrates [17, 23–25], which is more compatible with current silicon-based microelectronics technology. Compared with random networks of SWNT on substrates, the long parallel aligned SWNTs can avoid the overlap of the nanotubes and the resistance caused by the nanotube junctions; more importantly, they provide a controllable orientation for easy fabrication of multiple nanodevices with a possible consistent performance.

In this work, we firstly report that superlong well-oriented SWNT arrays can be generated by EtOH-CVD from rare earth metal Dy. The Raman spectroscopy with the combination of electrochemical deposition of Ag has been

Y. Qian (✉) · C. Wang · B. Huang
Department of Materials Science and Engineering,
East China Institute of Technology, Fuzhou 344000,
People's Republic of China
e-mail: yongqian006@sohu.com

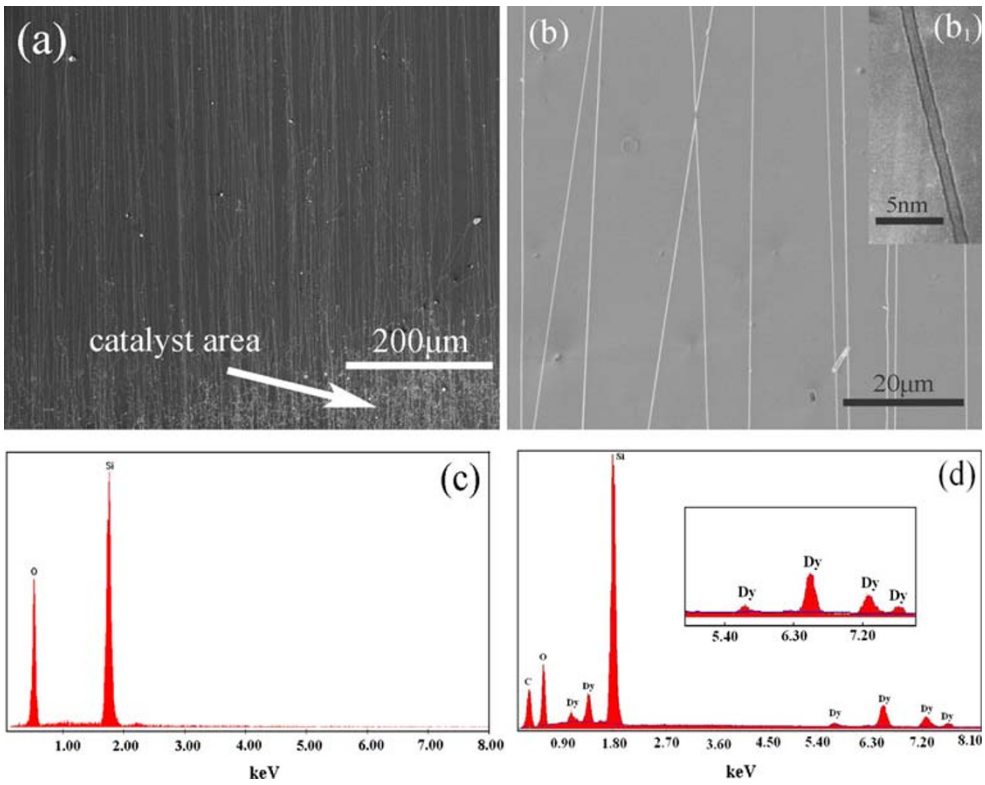

Fig. 1 **a** and **b** are SEM image and its part magnified image of well-oriented SWNT arrays on SiO_2/Si wafer, respectively; (b_1) is TEM image of individual nanotube; **c** and **d** are EDS spectra of the substrate before and after SWNT growth, respectively

applied to evaluate the structure of the as-grown SWNTs. This new element provides not only an alternative catalyst for the growth of SWNTs, but also a possible high percentage of superlong s-SWNT arrays for various SWNT-based nanodevice fabrications and applications.

Experimental

Superlong well-aligned SWNTs on SiO_2/Si wafer were grown by EtOH-CVD using 1 mM ethanol solution of dysprosium chloride ($DyCl_3$) that was purchased from Aldrich with purity higher than 99.99% as a catalyst precursor. The catalyst was loaded on one side of the substrate by dipping the wafer into catalyst-contained solution. The wafer was then placed in the middle of a 0.5-inch-diameter quartz tube within a 1-inch-diameter quartz tube in order to acquire laminar flow. After the furnace was heated to 900°C under the atmosphere of H_2 and Ar, ethanol vapor was delivered by bubbling H_2 (200 sccm) into ethanol with 1–3% water at 25–35°C. The growth lasted for 10 min.

In a typical experiment, the samples were dipped into the solution containing 0.1 mM $AgNO_3$ with 20 mM KNO_3 (analytical grade, Beijing reagents) as the supporting electrolyte. A saturated calomel electrode was used as the reference electrode, Pt gauze as counter electrode and long SWNT arrays connected by a conducting silver adhesive or Au layer by sputtering coating as a working electrode.

SEM images were taken from FEI NanoSEM at 1kv, spot 4,TEM images of SWNTs were taken from Si_3N_4 window where the nanotube grew in situ using a Philips CM200 TEM at 200 kV. AFM images were recorded at NanoScope III in tapping mode at room temperature, Raman spectra of SWNTs on silicon wafers were collected from JY-T64000 Raman spectroscopy under ambient conditions by using a laser excitation of 632.8 nm (1.96 eV, ~3 mw) or 514.5 nm (2.41 eV) from an air-cooled Ar^+ laser. The beam size is 2 μ.

Results and Discussion

Figure 1a shows the typical SEM image of the as-grown SWNT arrays and the catalyst area as indicated by arrow. The high magnification SEM image is showed in Fig. 1b, and the inset (Fig. $1b_1$) is TEM image. It can be seen from the SEM observation that the horizontally aligned SWNT arrays are uniform over a large area, and the density of the parallel SWNTs is about 3 –4 SWNTs/20 μm. Though this density is lower than those of aligned SWNT arrays grown on quartz [26] and sapphire [27], it is still very high among the reports of horizontally aligned arrays of SWNTs on silicon wafers [24, 25]. The length of the wafer is about

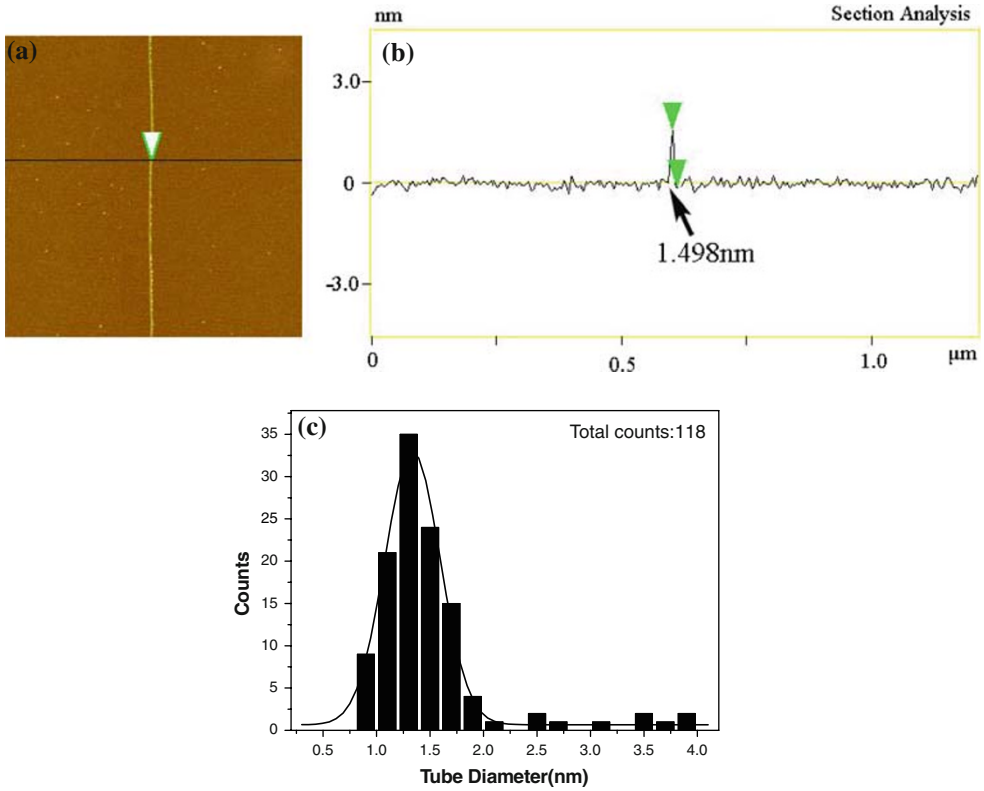

Fig. 2 **a** A representative AFM image of SWNTs at long oriented area; **b** the corresponding topographic height profile along the black line in part **a**; **c** diameter distribution of the SWNTs obtained from AFM measurements of 118 SWNTs. Gaussian fit is done and given the mean diameter of 1.336 nm

1.2 cm. Most of the nanotubes can grow from one side to another side of the wafer, indicating the length of the SWNT arrays in centimeter scale. Such large-area uniform SWNT arrays show attractive applications in various SWNT-based nanodevices. Figure 1c and d are typical EDS spectra of the SiO_2/Si substrate before and after SWNT growth, respectively, showing the presence of Dy. It is needed to point out that Fe, Co, Ni and any other metal elements are not found in the sample, indicating that it is Dy that acts as catalyst in the growth process.

The characterization of the nanotubes by AFM, TEM and Raman spectroscopy confirms their single-walled structure. Figure 2a presents a representative AFM image of long-oriented area. The corresponding topography height profile along the black line in Fig. 2a is shown in Fig. 2b. We can clearly see that the diameter of the SWNT is 1.498 nm that the black arrow indicates. On the basis of AFM measurements on 118 tubes, we obtain the diameter distribution of the SWNTs as shown in Fig. 2c. A Gaussian fit is done, and it gives the most probable diameter of 1.336 nm. Most of them have a diameter of less than 2.0 nm (108 tubes in 118, i.e., 91.5%). The diameter larger than 2.0 nm shown in part c is possibly related to small SWNT bundles or multi-walled carbon nanotubes. In addition, the mean diameter from TEM measurements of 93 SWNTs is 1.319 nm, which is slightly smaller than that of AFM.

Raman spectroscopy has been proven to be a powerful tool for characterizing and revealing the detailed structure and the electronic and phonon properties of SWNTs. As reported in our recent article [28, 29], it can be applied to characterize the carbon nanotubes in which the radial breathing model (RBM) can be used to identify the structure and the diameter (d) of the SWNT. The two different excitation frequencies of Raman lasers are taken from the same position of the as-grown SWNT arrays on SiO_2/Si wafer. The typical Raman spectra with the two different lasers are shown in Fig. 3. It can be seen that a strong G band peak at about 1594 cm^{-1} corresponds to graphitic structure, and a weak D band peak indicates a good quality of SWNTs. Furthermore, a RBM at around 194 cm^{-1} is observed. The diameter of the SWNT is calculated to be about 1.28 nm according to the equation of $d = 248\ cm^{-1}/\omega$ [30, 31], which is within the range obtained from our AFM and TEM observations.

To further investigate the quality of the SWNTs prepared with the Dy catalyst, a convenient and effective approach to identify the structures of superlong well-aligned SWNTs via the combination of electrodeposition of Ag particles on the SWNTs with Raman spectroscopy [28, 29]. We carried out typical electrochemical experiment in the horizontally long SWNT arrays. Such arrays make it possible for us to connect all the nanotubes with conducting metal, which can be used as an electrode for

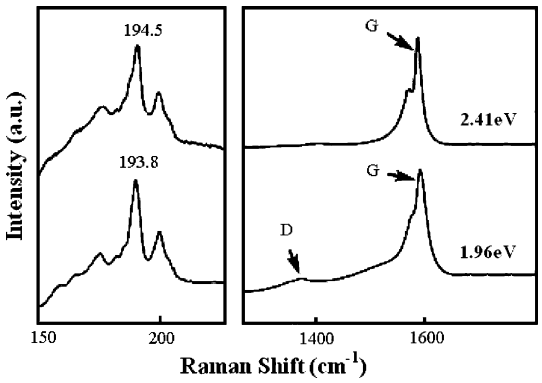

Fig. 3 Raman spectra for the same position of as-grown SWNT on SiO_2/Si wafer, measured using two laser excitations 2.41 and 1.96 eV. The left and right images are RBM and G band, respectively

deposition of metals. Figure 4a shows schematic representation of the three main processes in our experiment, from coating the catalyst precursor to horizontally aligned SWNT arrays grown to the electrodeposition of silver on SWNT arrays. Figure 4b is the SEM image showing the well-aligned SWNTs after electrodeposition of Ag for 10 s in 0.1 mM $AgNO_3$ solution at −0.6 V. It is interesting that the small amount of nanotubes do not have Ag deposition indicated by the black arrow in Fig. 4b. After careful checking with these long nanotubes, 457 out of 500 nanotubes are found to be deposited with Ag (91.4%), and only 8.6% SWNTs are without Ag deposition. While for superlong SWNT arrays from Fe/Mo and EtOH, 32% long SWNTs without Ag deposition was found [28]. The high percentage of SWNTs with Ag deposition from Dy and EtOH indicates that the SWNTs have better conductivity and better structural uniformity with fewer defects. For the nanotubes without Ag particles it is also easy to find out their location by using the nearby nanotubes with Ag particles and the edge of the electrode as a reference with the help of the SEM observation. It has been proven by the combination of electrochemical Ag deposition and Raman spectroscopy that the structure of an individual SWNT can be identified.

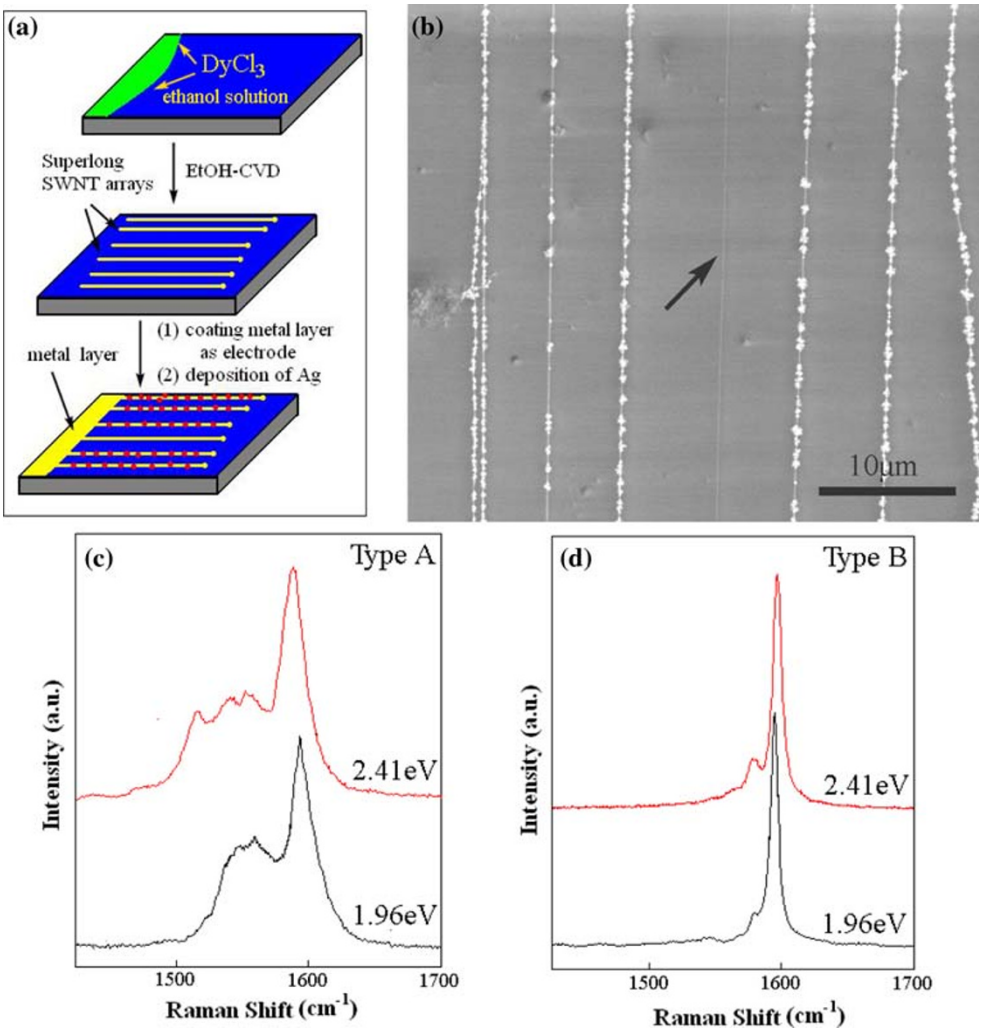

Fig. 4 **a** Schematic representation of the process from coating the catalyst precursor to the electrodeposition of silver on SWNT arrays. **b** SEM image of the superlong well-oriented SWNT arrays after Ag deposition. The SWNT without Ag deposition is indicated by the *black arrow*. **c** and **d** are typical Raman spectra (type *A*, *B*) from isolated individual SWNTs using two different laser excitations 2.41 and 1.96 eV

For superlong SWNTs from Dy and EtOH, we examined 93 individual, long nanotubes among which 85 nanotubes have Ag particles confirmed by Raman spectroscopy using 632.8 nm ($E_{laser} = 1.96$ eV) at 3 mw and found two different types of G band, type A and B, as shown in Fig. 4c and d. Nine nanotubes (9.7%) are type A that is typical m-SWNT with broad BWF and a Lorentzian peak around 1592 cm^{-1} (small shift for different nanotubes), and 72 nanotubes (77.4%) are typical s-SWNTs having strong sharp peaks at around 1594 cm^{-1} with a small peak at 1571 cm^{-1} (type B) that is typical s-SWNT. Eight nanotubes without Ag particles have possibly more defects along the nanotubes and behave as having an insulator character. In our recent article, we call them quasi-insulator nanotubes [28].

Since the Raman resonance of the SWNTs depends on both the excitation frequency and the diameter of the SWNT, it is necessary to use another laser line to identify the structures of the SWNTs. We further check the SWNTs by using Elaser 514.5 nm (Elaser = 2.41 eV) to collect the G band from 35 long tubes among which 32 nanotubes have Ag particles and find 4 m-SWNTs (11.4%) and 28 s-SWNTs (80%). The typical Raman spectra as shown in Fig. 4c and d. The percentage of the m-SWNTs measured from 514.4 nm excitation is similar to that from 632.8 nm excitation. Therefore, we could affirm that the well-aligned SWNTs from Dy catalyst with EtOH-CVD have a high percentage of s-SWNTs ($\sim$80%). A high percentage of s-SWNTs both vertically and horizontally aligned SWNT arrays on substrate have been reported more recently [32–34]. The horizontally aligned SWNT arrays can grow on ST-cut single-crystal quartz; the enrichment of s-SWNT (up to 95%) is believed to be due to the induced growth by the substrate lattice and the optimized growth condition. The reason for the growth of vertically aligned SWNT arrays with s-SWNT (up to 96%) still remains unclear. Further, more experiments need to be carried out for the better understanding of the mechanism of the preferential growth of s-SWNTs and the catalytic properties.

Conclusion

In summary, for the first time we have demonstrated that rare earth metal Dy is an effective catalyst for SWNTs growth. By using ethanol as carbon source, superlong well-oriented SWNT arrays can be generated. The results show that the SWNTs from Dy and EtOH have better conductivity and better structural uniformity with less defects. This new element provides not only an alternative catalyst for SWNTs growth, but also a way to generate high percentage of superlong s-SWNTs arrays. The generation of such high percentage of s-SWNT arrays will represent a big step forward in controlled growth of s-SWNTs for electronic applications.

Acknowledgments The authors would like to thank the MOST 973 project (2007CB616901) and NSFC (50772076) for their partial financial support.

References

1. S. Tans, A. Verschueren, C. Dekker, Nature **386**, 474 (1997)
2. C. Zhou, J. Kong, H. Dai, Appl. Phys. Lett. **76**, 1597 (2000)
3. Y. Yaish, J.Y. Park, S. Rosenblatt, V. Sazonova, M. Brink, Phys. Rev. Lett. **92**, 046401 (2004)
4. J. Kong, N. Franklin, C. Zhou, S. Pan, K. Cho, H. Dai, Science **287**, 622 (2000)
5. S. Iijima, T. Ichihashi, Nature **363**, 603 (1993)
6. D.S. Bethune, C.H. Kiang, M.S. de Vries, G. Gorman, R. Savoy, J. Vasquez, R. Beyers, Nature **363**, 605 (1999)
7. T. Guo, P. Nikolaev, A. Thess, D.T. Colbert, R.E. Smalley, Chem. Phys. Lett. **243**, 49 (1995)
8. H. Dai, A.G. Rinzler, P. Nikolaev, A. Thess, D.T. Colbert, R.E. Smalley, Chem. Phys. Lett. **260**, 471 (1996)
9. A.G. Nasibulin, A. Moisala, D.P. Brown, E.I. Kauppinen, Carbon **41**, 2711 (2003)
10. Y. Saito, Carbon **33**, 979 (1995)
11. J. Lu, S.S. Yi, T. Kopley, C. Qian, J. Liu, E. Gulari, J. Phys. Chem. B **110**, 6655 (2006)
12. W.Q. Deng, X. Xu, W.A. Goddard, Nano Lett. **4**, 2331 (2004)
13. L.H. Liang, F. Liu, D.X. Shi, W.M. Liu, X.C. Xie, H.J. Gao, Phys. ReV. B **72**, 35453 (2005)
14. D. Takagi, Y. Homma, H. Hibino, S. Suzuki, Y. Kobayashi, Nano Lett. **6**, 2642 (2006)
15. S. Bhaviripudi, E. Mile, S.A. Steiner, J. Kong, J. Am. Chem. Soc. **129**, 1516 (2007)
16. D. Takagi, Y. Kobayashi, H. Hibino, S. Suzuki, Y. Homma, Nano Lett. **8**, 832 (2008)
17. W. Zhou, Z. Han, J. Wang, Y. Zhang, Z. Jin, X. Sun, Nano Lett. **6**, 2987 (2006)
18. M. Ritschel, A. Lenonhardt, D. Elefant, S. Oswald, B. Büchner, J. Phys. Chem. C **111**, 8414 (2007)
19. Y. Zhang, W. Zhou, L. Ding, Z. Zhang, X. Liang, Y. Li, Chem. Mater. **20**, 7521 (2008)
20. H. Yoshida, S. Takeda, T. Uchiyama, H. Kohno, Y. Homma, Nano Lett. **8**, 2082 (2008)
21. D. Yuan, L. Ding, H. Chu, Y. Feng, T.P. McNicholas, J. Liu, Nano Lett. **8**, 2576 (2008)
22. B. Liu, W. Ren, L. Gao, S. Li, Q. Liu, H.M. Cheng, J. Phys. Chem. C **112**, 19231 (2008)
23. S.M. Huang, X.Y. Cai, J. Liu, J. Am. Chem. Soc. **125**, 5636 (2003)
24. L.M. Huang, X.D. Cui, B. White, S.P. O'Brien, J. Phys. Chem. B **108**, 16451 (2004)
25. S.M. Huang, M. Woodson, R.E. Smalley, J. Liu, Nano Lett. **4**, 1025 (2004)
26. C. Kocabas, S.H. Hur, A. Gaur, M.A. Meitl, M. Shim, J.A. Rogers, Small **1**, 1110 (2005)

27. S. Han, X. Liu, C. Zhou, J. Am. Chem. Soc. **127**, 5294 (2005)
28. S.M. Huang, Y. Qian, J.Y. Chen, Q.R. Cai, L. Wan, S. Wang, J. Am. Chem. Soc. **130**, 11860 (2008)
29. Y. Qian, S.M. Huang, F.L. Gao, Q.R. Cai, W.B. Hu, J. Phys. Chem. C **113**, 6983 (2009)
30. A. Jorio, R. Saito, J.H. Hafner, C.M. Lieber, Phys. Rev. Lett. **86**, 1118 (2001)
31. A. Jorio, C. Fantini, M.A. Pimenta, Phys. Rev. B **71**, 075401 (2005)
32. L. Qu, F. Du, L. Dai, Nano Lett. **8**, 2682 (2008)
33. L. Ding, A. Tselev, J. Wang, D. Yuan, H. Chu, T.P. McNicholas, Y. Li, J. Liu, Nano Lett. **9**, 800 (2009)
34. X. Wang, Q. Li, J. Jin, J. Wang, Y. Li, K. Jiang, S. Fan, Nano Lett. **9**, 3137 (2009)